

Article

Varying Performance of Low-Cost Sensors During Seasonal Smog Events in Moravian-Silesian Region

Václav Nevrlý^{1,2,*}, Michal Dostál^{1,2}, Petr Bitala¹, Vít Klečka¹, Jiří Sléžka¹, Pavel Polách¹, Katarína Nevrlá¹, Melánie Barabášová¹, Růžena Langová¹, Šárka Bernatíková¹, Barbora Martiníková¹, Michal Vašínek³, Adam Nevrlý³, Milan Lazecký⁴, Jan Suchánek², Hana Chaloupecká⁵, David Kiča⁶ and Jan Wild¹

- ¹ Faculty of Safety Engineering, VSB-Technical University of Ostrava, Lumírova 630/13, 700 30 Ostrava-Výškovice, Czech Republic; michal.dostal1@vsb.cz (M.D.); petr.bitala@vsb.cz (P.B.); vit.klecka@vsb.cz (V.K.); melanie.barabasova@vsb.cz (M.B.); ruzena.langova@vsb.cz (R.L.); sarka.bernatikova@vsb.cz (Š.B.); barbora.martinikova@vsb.cz (B.M.); jan.wild@vsb.cz (J.W.)
- ² J. Heyrovský Institute of Physical Chemistry, Czech Academy of Sciences, Dolejškova 2155/3, 8, 182 23 Praha, Czech Republic; jan.suchanek@jh-inst.cas.cz
- ³ Faculty of Electrical Engineering and Computer Science, VSB-Technical University of Ostrava, 17. Listopadu 15/2172, 708 00 Ostrava-Poruba, Czech Republic
- ⁴ IT4Innovations, VSB—Technical University of Ostrava, 17. Listopadu 15/2172, 708 00 Ostrava-Poruba, Czech Republic
- ⁵ Institute of Thermomechanics of the Czech Academy of Sciences, Dolejškova 5, 8, 182 00 Praha, Czech Republic; hana.chaloupecka@it.cas.cz
- ⁶ Public Health Institute Ostrava, Partyzánské Náměstí 2633/7, Moravská Ostrava, 702 00 Ostrava, Czech Republic
- * Correspondence: vaclav.nevrlly@vsb.cz; Tel.: +420-59-732-2872



Citation: Nevrlý, V.; Dostál, M.; Bitala, P.; Klečka, V.; Sléžka, J.; Polách, P.; Nevrlá, K.; Barabášová, M.; Langová, R.; Bernatíková, S.; et al. Varying Performance of Low-Cost Sensors During Seasonal Smog Events in Moravian-Silesian Region. *Atmosphere* **2024**, *15*, 1326. <https://doi.org/10.3390/atmos15111326>

Academic Editors: Carla Gamelas and Nuno Canha

Received: 1 October 2024

Revised: 26 October 2024

Accepted: 31 October 2024

Published: 3 November 2024



Copyright: © 2024 by the authors. Licensee MDPI, Basel, Switzerland. This article is an open access article distributed under the terms and conditions of the Creative Commons Attribution (CC BY) license (<https://creativecommons.org/licenses/by/4.0/>).

Abstract: Air pollution monitoring in industrial regions like Moravia-Silesia faces challenges due to complex environmental conditions. Low-cost sensors offer a promising, cost-effective alternative for supplementing data from regulatory-grade air quality monitoring stations. This study evaluates the accuracy and reliability of a prototype node containing low-cost sensors for carbon monoxide (CO) and particulate matter (PM), specifically tailored for the local conditions of the Moravian-Silesian Region during winter and spring periods. An analysis of the reference data observed during the winter evaluation period showed a strong positive correlation between PM, CO, and NO₂ concentrations, attributable to common pollution sources under low ambient temperature conditions and increased local heating activity. The Sensirion SPS30 sensor exhibited high linearity during the winter period but showed a systematic positive bias in PM₁₀ readings during Polish smog episodes, likely due to fine particles from domestic heating. Conversely, during Saharan dust storm episodes, the sensor showed a negative bias, underestimating PM₁₀ levels due to the prevalence of coarse particles. Calibration adjustments, based on the PM₁/PM₁₀ ratio derived from Alphasense OPC-N3 data, were initially explored to reduce these biases. For the first time, this study quantifies the influence of particle size distribution on the SPS30 sensor's response during smog episodes of varying origin, under the given local and seasonal conditions. In addition to sensor evaluation, we analyzed the potential use of data from the Copernicus Atmospheric Monitoring Service (CAMS) as an alternative to increasing sensor complexity. Our findings suggest that, with appropriate calibration, selected low-cost sensors can provide reliable data for monitoring air pollution episodes in the Moravian-Silesian Region and may also be used for future adjustments of CAMS model predictions.

Keywords: air quality; low-cost sensors; Polish smog; Saharan dust storm; linear regression

1. Introduction

The Moravian-Silesian Region in the Czech Republic, particularly the city of Ostrava, is recognized as a significant air pollution hot spot in Europe. This situation arises historically

from a combination of industrial activity, high population density, and geographical factors that worsen air quality levels. The topography of the Moravian-Silesian Region contributes to the accumulation of pollutants, especially during winter months when temperature inversions are common. This leads to poor dispersion, resulting in elevated concentrations of air pollutants. Additionally, air pollution from neighboring areas, particularly from the Silesian Voivodeship (Poland), also plays a significant role in the given context [1–3].

Recently, “Polish smog” was proposed as a specific type of air pollution that occurs in Poland, particularly in the winter months. It is characterized by high concentrations of particulate matter (PM), such as PM_{2.5} and PM₁₀, as well as polycyclic aromatic hydrocarbons like benzo(a)pyrene with adverse health effects [4]. This type of smog is particularly prevalent in Eastern Europe, where it arises from the burning of coal and other solid fuels for heating purposes, especially during the winter months. When compared with photochemical smog found in industrialized urban areas, which is driven mainly by volatile organic compounds (VOCs) and nitrogen oxides leading to high ozone levels, Polish smog is more closely linked to residential heating practices and industrial emissions [5].

Yet, another type of smog event, which is further considered throughout this paper, is caused by particulate matter originating from Sahara desert. Dust storms can transport particles over thousands of kilometers, affecting air quality far from their source. The transport of Saharan dust poses significant challenges for air quality management and public health in Europe. Although this phenomenon is more common in the Mediterranean region, it can occasionally cause a significant deterioration in air quality for Central European countries.

Low-cost sensor (LCS) networks have emerged as a promising solution for monitoring air pollution and providing smog alerts as they can supplement data from regulatory-grade reference instruments [6]. By filling in spatial and temporal gaps in air quality monitoring, such information can provide a more comprehensive understanding of pollution patterns both at local and regional level. Citizen science projects involving the public in sensor deployment can further expand the reach of these networks [7–9]. However, the proper calibration of LCSs is crucial to ensure data accuracy and reliability [10].

In principle, uncertainties of factory-calibrated LCS response are studied by experiments in controlled (laboratory) or uncontrolled (field) ambient conditions [11–13]. Such a calibration procedure is followed by a selection of suitable numerical correction methods and an estimation of parameters using reference datasets for model training or testing purposes [14]. The co-location of the LCS node with reference instruments in real outdoor atmosphere is usually performed over a period of several weeks in order to accumulate appropriately large datasets required for the reliable outputs of the calibration process. A prolonged period of co-location enables us to investigate the seasonal variability of LCS performance across a wide range of environmental conditions relevant for the target locality.

In the given context, our study focuses on three key objectives related to the performance and application of an LCS network in the Moravian-Silesian Region:

Aim 1 is to evaluate the accuracy and reliability of a prototype sensor node specifically designed for local conditions in the region, focusing on the winter and spring periods. This study analyzes the data obtained from low-cost sensors, particularly the Sensirion SPS30 and Alphasense CO-B4 sensors, and compares them with data from regulatory AQM stations to evaluate sensor accuracy in detecting PM and CO during air pollution episodes. Aim 2 is to investigate whether and how the reliability of the SPS30 sensor can be enhanced under local conditions. While the SPS30 sensor has shown promise in monitoring particulate matter, it also presents limitations, particularly in its ability to accurately measure larger particles, such as PM₁₀. This study explores potential calibration improvements, including corrections based on particle size distribution, to address the observed biases in PM₁₀ measurements.

Aim 3 is to analyze the potential use of data from the Copernicus Atmospheric Monitoring Service (CAMS) as an alternative to increasing the complexity of the LCS node. The CAMS provides regional air quality forecasts, including PM₁₀ and CO concentrations, which

could potentially complement or replace the need for additional sensors in the low-cost monitoring framework.

Overall, the goal of our research is to develop a new framework for data analysis and practical guidance for the calibration of low-cost sensors in urban air pollution environments by combining observations from AQM stations and CAMS model predictions. In particular, we aim to provide new insights into the reliability of the SPS30 sensor for further use in citizen science-based air quality monitoring initiatives, which has been critically discussed in the recent literature, e.g., [15].

2. Materials and Methods

Our prototype LCS sensor node (more details are described in Appendix A) was mounted on the roof of the AQM station (see Figure 1). This setup allows for a direct comparison between the outputs of the LCS node and data from reference-grade instruments.



Figure 1. LCS sensor node placed on the roof of the reference air quality monitoring station of the health institute in Ostrava located in the Mariánské Hory district.

2.1. Selection of Low-Cost Sensors

Following our goals, the LCS node is equipped with a set of low-cost sensors suitable for the monitoring of primary air pollutants for the specific area, which are particulate matter (PM) and carbon monoxide (CO). The selection of the gas and PM sensors was mainly based on the extensive literature survey and experience of previous investigators. The availability of the sensors (their distribution in the EU) was also taken into account as well as the affordability of the entire LCS node setup and level of complexity relevant to the requirements for its integration and further development.

For the particulate matter (PM) measurement, the node utilizes a pair of commercially available sensors: Sensirion SPS30 and Alphasense OPC-N3. The SPS30 is a laser-based optical sensor well suited for measuring fine particulate matter (especially PM_{10}) mass concentration based on the principle of light scattering. The OPC-N3 also uses optical particle counting when detecting a wider range of particle sizes, from $0.35 \mu m$ to $40 \mu m$, across 24 size bins, enabling particle size distribution to be determined, which is critical for understanding the composition of atmospheric aerosols and the determination of their origin in relation to source apportionment.

For carbon monoxide monitoring, the LCS node incorporates the Alphasense CO-B4 electrochemical sensor. This sensor can detect CO concentrations between 0 and 1000 ppm, with a resolution of 0.1 ppm. Its sensitivity ranges from 55 to 85 nA/ppm, providing an accurate detection of small changes in CO levels.

Knowledge of ambient temperature and relative humidity (RH) is essential when aiming at corrections of LCS response in various ambient conditions. For this purpose, a digital module including the Bosch Sensortech BME280 sensor was integrated into the LCS node. This sensor operates with a temperature accuracy of ± 1 °C and a humidity accuracy of $\pm 3\%$ RH.

2.2. Co-Location Site and Reference Instruments

The co-location measurements of the LCS node were conducted at an air quality monitoring (AQM) station of the health institute located in the municipal area of the city of Ostrava, which is close to various industrial sites (e.g., metallurgical, chemical, etc.). The AQM station provides information on meteorological conditions, such as wind speed and direction, as well as reference air quality data in hourly intervals. Atmospheric pressure, temperature, and humidity are measured using the COMET T3113D sensor for temperature and humidity, and the NXP Semiconductor MPX4115A for pressure. For CO measurements, an HORIBA APMA-370 analyzer is used. The station also monitors nitrogen dioxide (NO₂) with the HORIBA APNA-370 analyzer and ozone (O₃) with the HORIBA APOA-370 analyzer. A TEOM 1400 analyzer was used as a reference for PM₁₀ during the entire winter evaluation period, including the S1 episode. At the end of March 2024, the TEOM 1400 was replaced by a Palas FIDAS 200 analyzer, which provides continuous real-time reference measurements of size distribution, allowing the quantification of PM₁, PM_{2.5}, and PM₁₀. Detection principles for each measurement are detailed in Table 1.

Table 1. Reference methods and detection limits of the instrumentation available at the AQM station.

Measurement Target	Principle	Limit of Detection
Carbon monoxide (CO)	Non-Dispersive IR Spectrometry	200 µg/m ³
Ozone (O ₃)	UV Photometry	10 µg/m ³
Nitrogen dioxide (NO ₂)	Chemiluminescence	8 µg/m ³
Particulate matter (TEOM)	Oscillating Microbalance	5 µg/m ³
Particulate matter (FIDAS)	Optical Scattering	1 µg/m ³
Ambient temperature	On-Chip Electronics	± 1 °C
Relative humidity	On-Chip Electronics	$\pm 3\%$
Atmospheric pressure	On-Chip Electronics	± 1 hPa

2.3. Overview of Co-Location Measurement

Low-cost sensors are often collocated with reference instruments in laboratory or field conditions for a period of several weeks in order to improve their performance. In our case, an evaluation measurement campaign lasting for three months (from mid-November 2023 to mid-February 2024) was initially planned to be carried out in order to verify and validate the performance of individual LCSs and their variation for seasonal meteorological conditions typical in the Moravian-Silesian Region.

Additionally, smog alert events, which occurred in Ostrava during December 2023 and April 2024, were also recorded during an extended period of co-location. These datasets enabled us to focus our attention on the performance of LCS and CAMS data versus reference measurements during the episodes of serious air quality deterioration (see Table 2).

Table 2. Smog episodes with relative humidity, temperature and pressure characterized by their mean and standard deviation values (in brackets).

Period	Start	End	Hum. (%)	Temp. (°C)	Pres. (hPa)
S1	5 December 2023	9 December 2023	98(±2)	−2(±2)	1016(±3)
S2	29 March 2024	2 April 2024	45(±15)	15(±10)	1004(±4)

In general, the differences in meteorological conditions between S1 and S2 are mostly due to the distinct seasonal conditions of Central Europe. Specifically, S1 is associated with high atmospheric stability and the inflow of cold and wet air masses typical for continental weather during the winter season, while S2 is characterized by a long-range (i.e., inter-continental) transport of dry and warm air from the south via the so-called “Moravian Gate”, associated with relatively higher wind speeds.

It is worth noting that atmospheric conditions for the S1 episode are typical for the above-mentioned “Polish smog”. In the given case the highest concentrations of particulate matter are generally recorded at low temperatures, specifically between -10 °C and 0 °C . Additionally, higher atmospheric pressure correlates with increased PM concentrations, as stable air masses inhibit vertical mixing and allow pollutants to accumulate near the surface [5]. The evolution of the above-described meteorological situation can be identified from Figure 2 based on reference data from the AQM station.

Different atmospheric conditions for the S2 episode corresponds to the seasonal Saharan dust storm over Central Europe (for more detailed information on the given topic, see (accessed on 1 September 2024) the following text available online: <https://atmosphere.copernicus.eu/climate-atmosphere-podcast-understanding-impact-saharan-dust-storms>). A moderate speed of the wind blowing from the south-west direction can be clearly identified during PM_{10} maxima from Figure 2.

2.4. Datasets and Preparatory Analysis

Following the aims of this study, we utilized three sets of time series to evaluate the LCS measurements and analyze the data, whose contents and temporal resolution are illustrated in Figure 3. These data (including the interactive Python notebooks), enabling their processing and analysis, are fully available from the public repository mentioned in the Data Availability Statement.

Datasets extracted from the LCS node were converted into hourly time series using the pandas (Python library) resample method and ordered with the reference and CAMS model data according to relevant GMT timestamps.

Reference AQM data were extracted from datasets provided by the health institute (the AQM station) after their verification involving the replacement of values of measurements below the limit of detection (LoD , see Table 1) by the value equal to $LoD/2$.

Site-specific time series of concentrations for the selected pollutant (CO , O_3 , NO_2 , PM_{10} , $\text{PM}_{2.5}$ and Dust) based on the forecast of the CAMS ENSAMBLE model [16] with 11 km spatial resolution were downloaded in the form of comma-separated value (CSV) files from the Open Meteo (<https://open-meteo.com/>) webpage.

The CAMS ENSAMBLE model provides daily high-resolution air quality analyses and forecasts for Europe. It utilizes an ensemble of eleven air quality forecasting systems, generating a median ensemble from individual model outputs to enhance predictive performance. This approach allows for better uncertainty estimation based on the variability among the models. Data assimilation techniques integrate model outputs with observations from the European Environment Agency (EEA), creating a comprehensive dataset. Forecasts are produced daily for the next four days, available at hourly intervals and multiple vertical levels. Practical implementation on the CAMS for urban air quality monitoring and more detailed information concerning the model predictions are described, e.g., in [17].

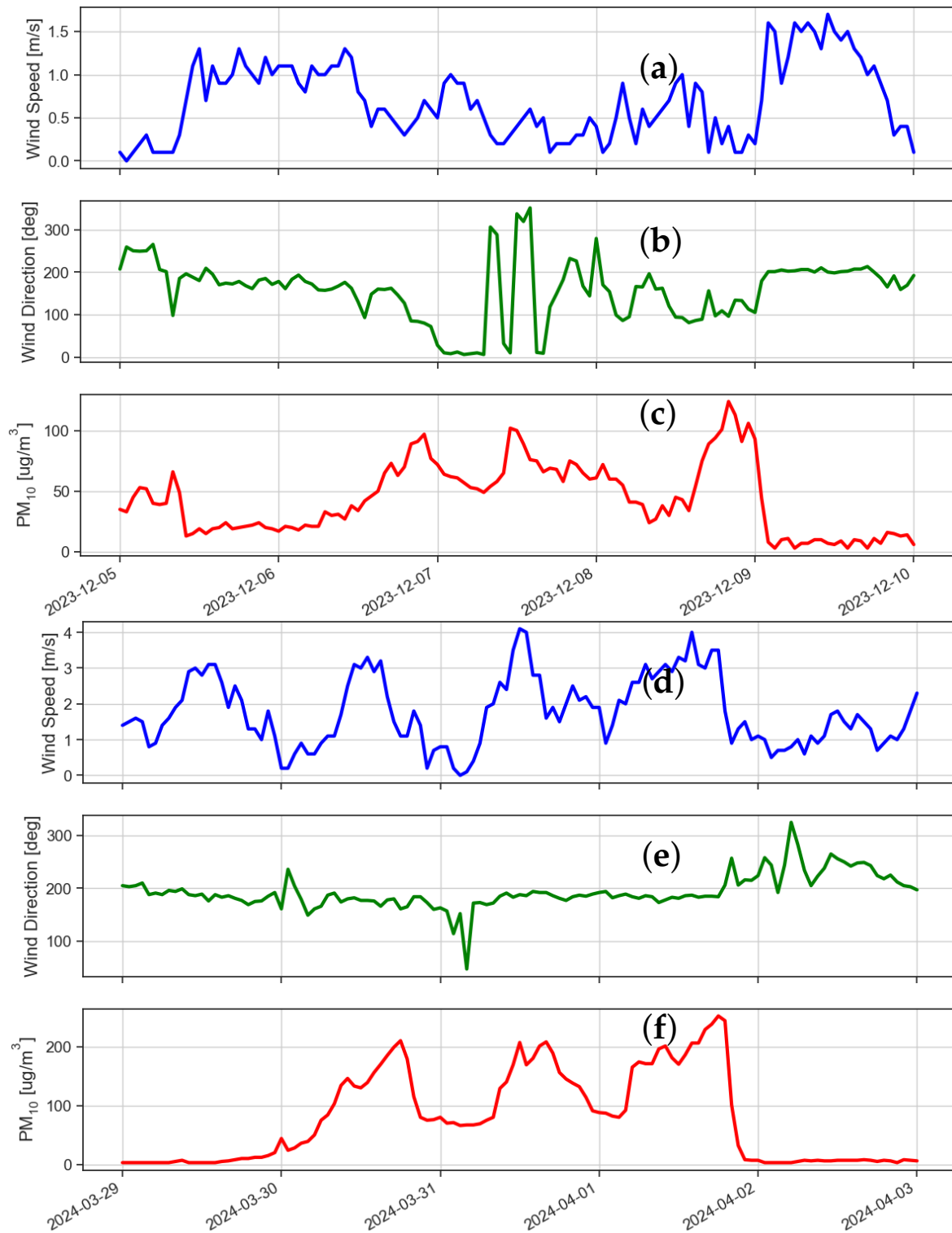


Figure 2. Temporal evolution of wind speed, wind direction, and reference particulate matter $[PM_{10}]_{REF}$ concentrations during S1 (a–c) and S2 (d–f) episodes, respectively. Wind direction in degrees indicates the origin of the wind ($0^\circ = 360^\circ =$ north, $90^\circ =$ east, $180^\circ =$ south, $270^\circ =$ west).

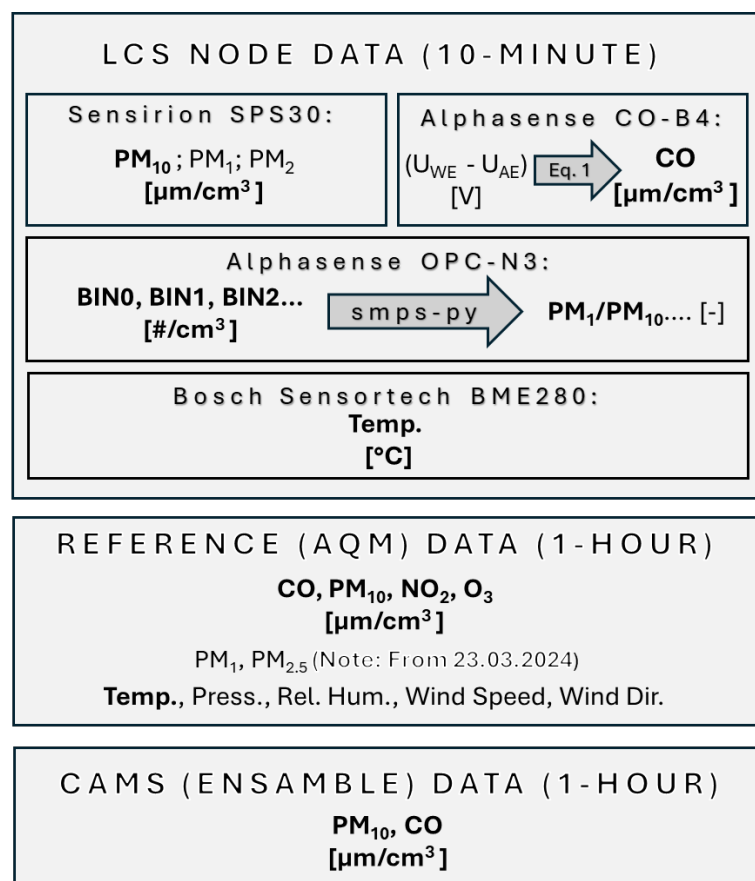


Figure 3. Schematic representation of datasets and quantities used for exploratory and regression data analyses (in bold) with corresponding temporal resolution. These datasets as well as data processing tools (including interactive Python notebooks) are available at the Zenodo repository (see the Data Availability Statement).

The multilinear fitting (MLR) values of the carbon monoxide LCS voltage were converted into concentration using linear model form `scikit-learn` (Python library). The entire dataset of winter measurements, i.e., from November 2023 to February 2024, was assumed as a representative for the given step. Temperature readings from the LCS node were converted into Kelvins in order to avoid numerical issues relevant to negative values. The entire dataset was split into training and testing subsets, with 1232 and 2392 data points, respectively. Finally, the MLR model, with a high coefficient of determination, i.e., $R^2 = 0.89$, and acceptable mean average error (MAE $< 50 \mu g/m^3$) for the predicted CO concentration was estimated assuming only $T[K]$ and CO-B4 sensor voltage values as predictors with the presumed parametrization of Equation (1)

$$[CO]_{LCS}(\tau) = c_1 \times [U_{WE}(\tau) - U_{AE}(\tau)] + c_2 \times T(\tau) + c_3 \quad (1)$$

where $U_{WE}(\tau)$ is a working electrode voltage [V], $U_{AE}(\tau)$ is an auxiliary electrode voltage [V] at given Greenwich (i.e., GMT) time τ and case-specific values of relevant MLR coefficients are as follows: $c_1 = 4394$ and $c_2 = -0.693$, $c_3 = 0$.

An exploratory data analysis including Correlation Matrix and Kernel Density Estimation (KDE) of dataset pairs was performed using `seaborn` (Python library). Subsequently, simple linear regression (SLR) and plots of diurnal variations in air pollutant concentrations were performed employing the relevant methods implemented in `atmospy` (Python library). Particle size distribution measured by the Alphasense OPC-N3 sensor was analyzed using the `smps-py` (Python library).

3. Results

3.1. Key Findings from Winter Evaluation Period

In winter, the time series for key air pollutants were expected to be significantly correlated, which was confirmed from the analysis of the reference data (PM₁₀, CO, NO₂, and O₃). The correlation between the given variables was quantified using the Pearson correlation coefficient, which measures the strength of a linear relationship between two variables, x and y . This coefficient (r) was calculated using Equation (2):

$$r = \frac{\sum(x_i - \bar{x})(y_i - \bar{y})}{\sqrt{\sum(x_i - \bar{x})^2 \sum(y_i - \bar{y})^2}}, \quad (2)$$

where index i represents the i -th data point in the reference dataset. Carbon monoxide shows a strong positive correlation with PM₁₀, with a Pearson coefficient value of $r = 0.85$, as shown in Figure 4, which can be attributed to a similar source of these pollutants or to a related mechanism, e.g., atmospheric dispersion.

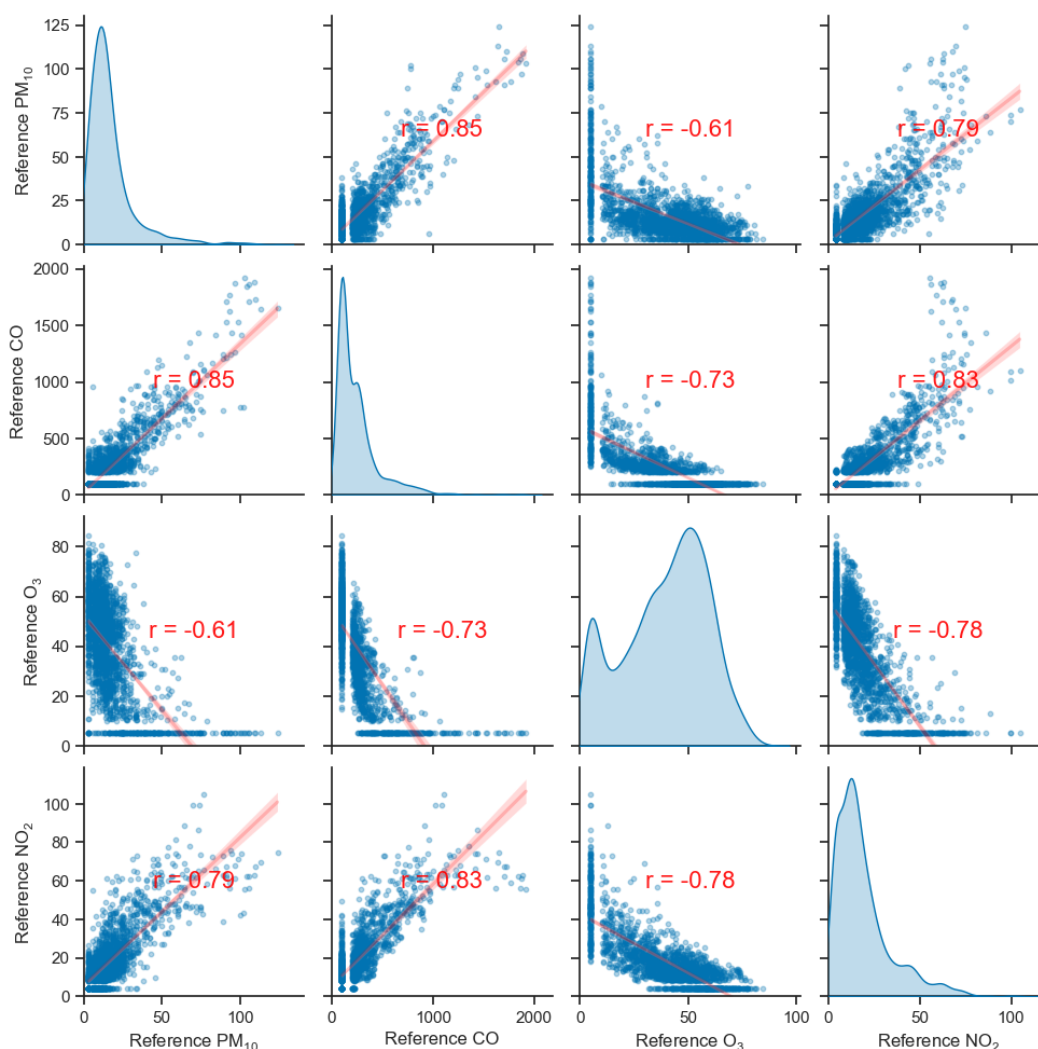


Figure 4. The correlation matrix with scatter plots, linear regression and probability density functions (PDFs) for reference pollutant concentrations from the winter evaluation period. The diagonal subplots displaying the PDFs of the variables are depicted on a relative scale. Note that the area under each PDF curve equals 1, indicating the total probability. All scales for non-diagonal subplots are depicted in [$\mu\text{g}/\text{m}^3$] units. Pearson correlation coefficients r and relevant linear regression lines are depicted in red.

At the same time, the NO_2 concentration values are also correlated with CO and PM_{10} . This observation is in line with an assumption that the incomplete combustion of fossil fuels, and subsequent atmospheric dispersion of smoke plumes, is a dominant contributor to winter air pollution in the given location. As can be expected, due to the lower solar (UV) radiation intensity, ozone concentrations only rarely reached elevated values (above $75 \mu\text{g}/\text{m}^3$) during this period. The negative correlation of O_3 with concentrations of other pollutants can be explained by a combination of meteorological factors, i.e., higher atmospheric stability, which prevents the vertical dispersion of ozone in winter, and reduced ozone formation reaction rates due to lower ambient temperature and reduced photochemical activity. Other factors mentioned in the literature [18] are the reduced intensity of solar radiation over the ground in the presence of high particle concentrations, as well as the shift in the chemical equilibrium towards ozone consumption at high levels of NO_2 in the atmosphere.

The most prominent qualitative features of the LCS response and selected CAMS model predictions can be recognised from the plots of the selected hourly data (Figure 5), when compared to the reference measurements. Firstly, we can spot the excellent fit of $[\text{CO}]_{\text{LCS}}$ to $[\text{CO}]_{\text{REF}}$, together with the systematic shift of $[\text{CO}]_{\text{CAMS}}$ data towards slightly higher values. On the contrary, the PM_{10} response provided by the SPS30 sensor is considerably overestimated (especially for $\text{PM}_{10} > 50 \mu\text{g}/\text{m}^3$) compared to the PM_{10} prediction by the CAMS model, which is very close to the reference data.

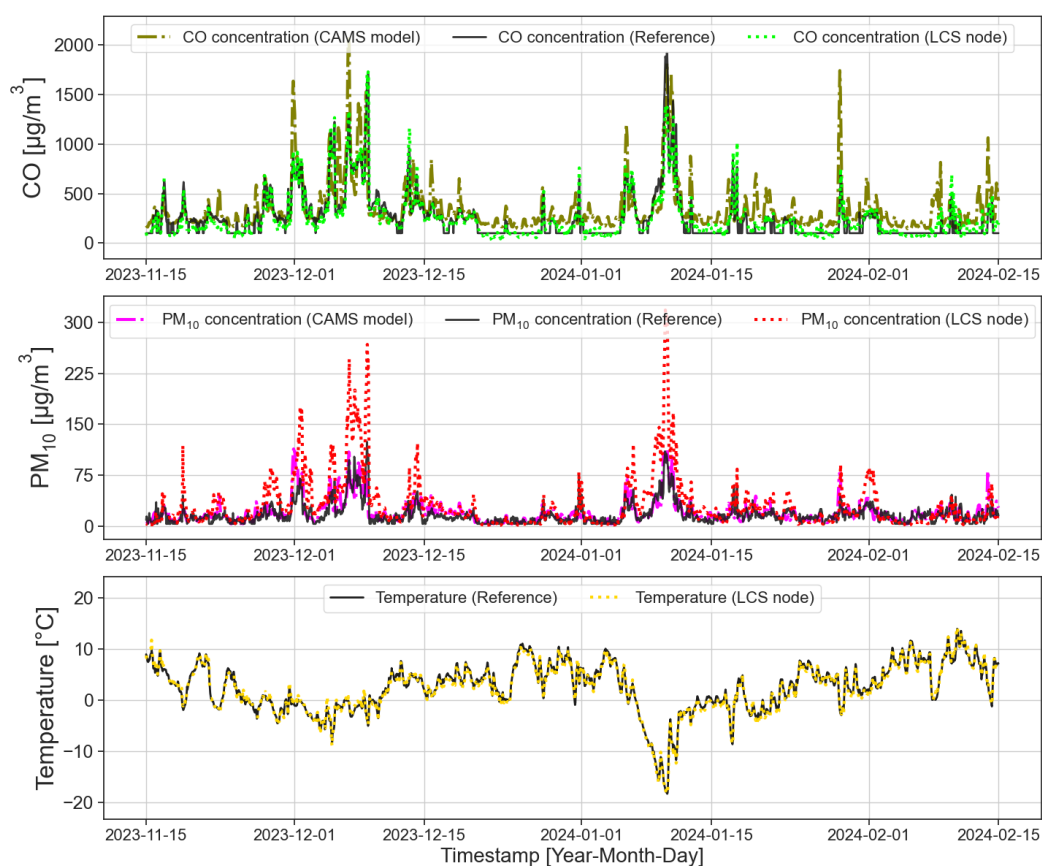


Figure 5. Comparison of the selected hourly data series from winter evaluation period.

A significant correlation of the main pollutants with reduced ambient temperature is confirmed by negative Pearson coefficients for PM_{10} ($r = -0.42$), CO ($r = -0.56$) as well as NO_2 ($r = -0.51$). Numerous spikes in CO and PM_{10} time series follow a sharp decrease in ambient temperature (mostly below $0 \text{ }^\circ\text{C}$). We can also discern the excellent agreement of temperature from the LCS node with the reference data, which is important due to the requirement of correcting the CO-B4 sensor according to Equation (1).

The overall quality of the LCS node data and the qualitative indicators of the CAMS model compared to the reference measurements are also illustrated by the plots shown in Figure 6. The average reference CO concentration over the evaluation period shows the same trend of diurnal variation as PM_{10} .

In the case of carbon monoxide, the LCS data show a nearly perfect correlation with the reference diurnal trend. There is obvious increase in CO and PM_{10} during morning rush hours (at about 8 A.M.) and a second peak around 8 P.M. Conversely, for the morning peak, the $[PM_{10}]_{CAMS}$ value (predicted by the CAMS) coincides with the reference measurement of PM_{10} ($[PM_{10}]_{REF}$).

The peak PM_{10} concentration predicted in the late evening hours by the CAMS model is significantly overestimated in a similar way to that observed in the diurnal plot for CO. This may be related to the uncertainty in the CAMS model input data regarding emission factors from industrial sources or domestic heating. For example, the Czech Republic is currently undergoing technological improvements based on government support for the replacement of domestic heating systems, which may have already been effective but has not yet been reflected in the model inputs. The plot of the diurnal SPS30 response, i.e., $[PM_{10}]_{LCS}$, shows a large overestimation with a more pronounced deviation during the night hours.

In the following sections of this paper, we anticipate that this change is due to a combination of the specific sensitivity of the SPS30 sensor and the changing ratio of fine to coarse particles in the air over the course of the day and year due to different intensities of domestic and industrial combustion and smoke dispersion (see Section 4).

Prior to the start of this study, we assumed that the Alphasense OPC-N3 sensor integrated in the LCS node would be used to accurately determine PM concentrations as a complementary measurement to the TEOM reference. However, it has been found that the OPC-N3 response does not show adequate agreement with the reference instrument ($R^2 < 0.3$ for PM_{10} for the evaluation period). Nevertheless, the particle size distribution was continuously measured by this sensor throughout the co-location period. Thus we used these data to determine the particle size-resolved spectra. Particle volume concentrations for each of the 24 bins were determined from measured values (i.e., the number of particles counted per sensor bin) and their daily mean values were recalculated.

In the next step, we expressed monthly averaged values for each bin to examine whether our data showed a seasonal trend. As can be seen in Figure 7, where the normalized particle size distributions are plotted, there is a clear predominance of submicron particles during the so-called heating season, which is less pronounced in February, as this month is exceptionally warm in the corresponding year compared to previous temperature records. Thus, the PM_1/PM_{10} ratio equal to 0.26 is consistent with a lower heating intensity and suggests that our assumptions regarding the influence of local combustion processes on the particle size distribution are correct.

3.2. LCS Performance During Polish Smog

Figure 8 shows a highly linear response of the CO-B4 sensor during the S1 episode. The slope parameter is nearly equal to its value obtained for the entire evaluation period. This fact can be expected due to the large span of data points from low to high CO concentration values recorded during the smog episode. However, we can find a close agreement of the data with the initial $[CO]_{LCS}$ calibration according to Equation (1). Note that the data points recorded, when the values measured by the reference instrument were below the detection limit (i.e., $[CO]_{REF} < 200 \mu\text{g}/\text{m}^3$), were removed before the SLR analysis.

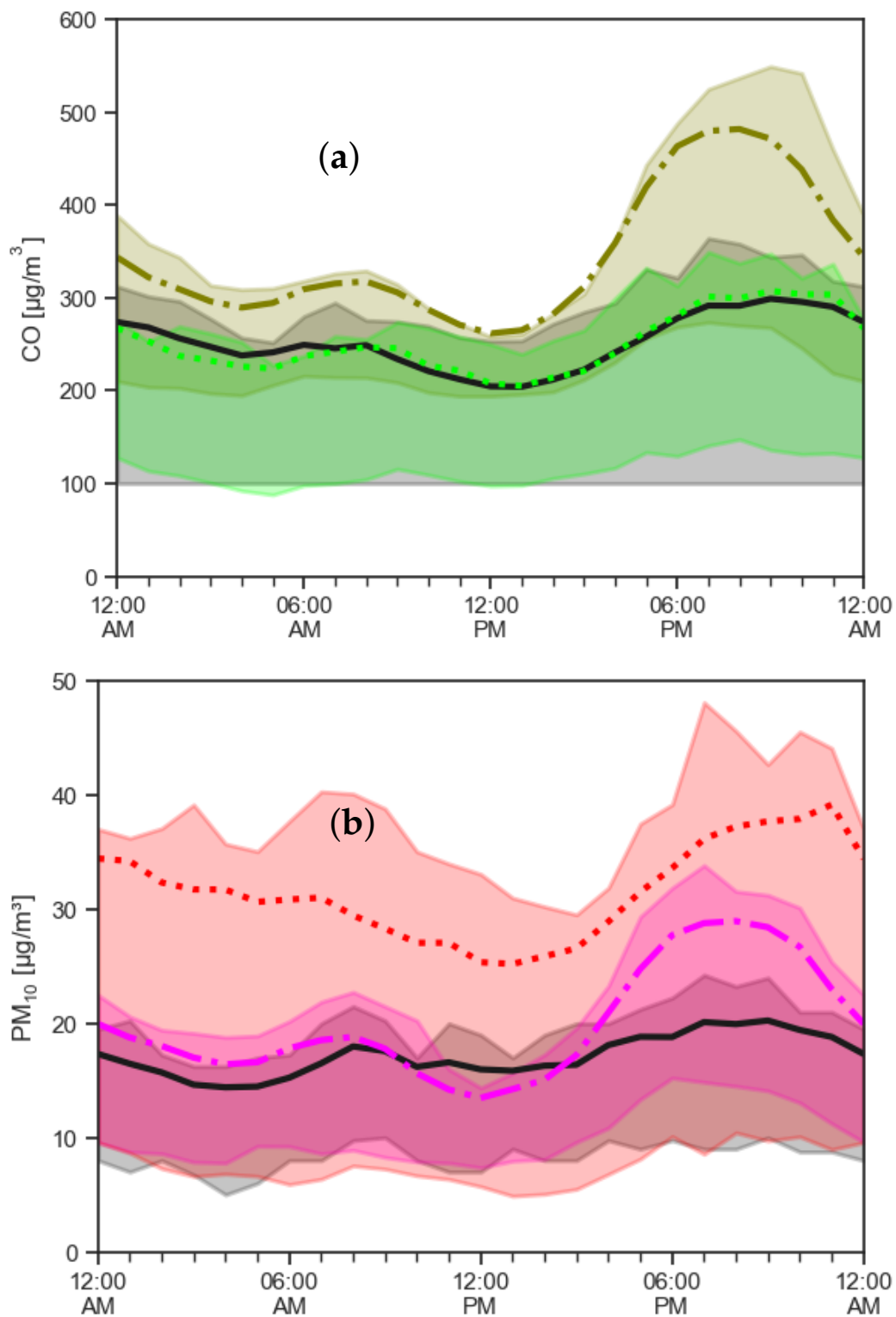


Figure 6. Plot of diurnal variations in CO concentration (a) and PM_{10} (b) during winter evaluation period, extracted from reference instrument (solid line), LCS node (dotted line) and CAMS model (dash-dotted line) data, with mean value (thick lines) and the interquartile range (shaded regions).

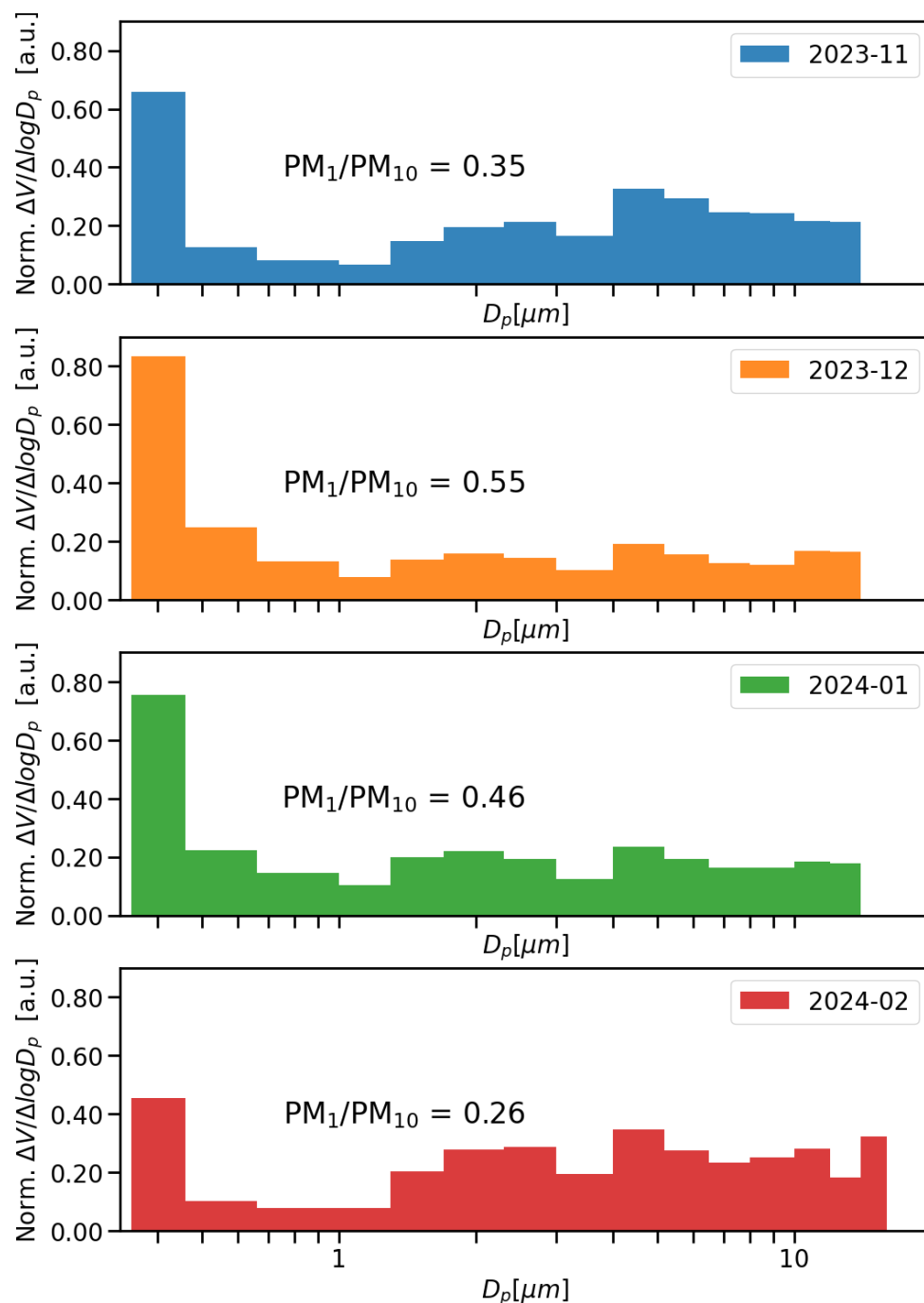


Figure 7. The seasonal variation in size distribution depicted as the normalized particle volume by bin of the Alphasense OPC-N3 sensor. The value of mass-weighted PM_1/PM_{10} ratio was estimated for each co-location month, based on the median value of the relevant 24 h averages.

Systematically, an over-predicted PM_{10} response was obtained from the SPS30 sensor compared to the TEOM reference instrument during the S1 episode. Nevertheless, a similar value of slope parameter a was obtained from the SLR fit (where a is the slope of the $y = ax + b$ regression line) for the entire winter evaluation period (see Figure 9). These results indicate the consistency of datasets obtained from the SPS30 sensor response, together with a relatively high coefficient of determination ($R^2 > 0.8$) for PM_{10} over the entire co-location period.

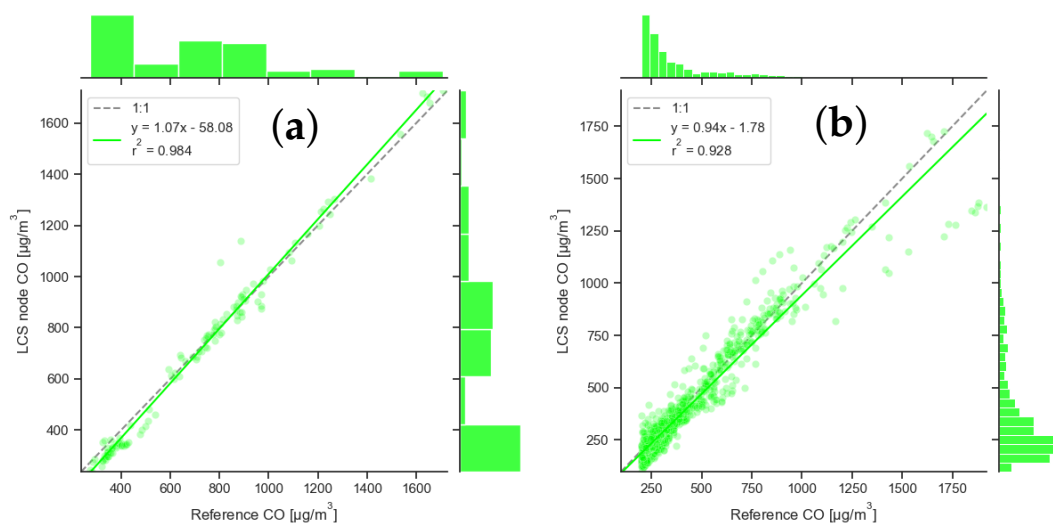


Figure 8. Simple linear regression of Alphasense CO-B4 sensor response versus reference instrument (HORIBA) for “Polish smog” episode S1 (a) compared with data for winter evaluation period (b). Histograms displayed adjacent to axes illustrate normalized frequency of measured concentration ranges within respective dataset.

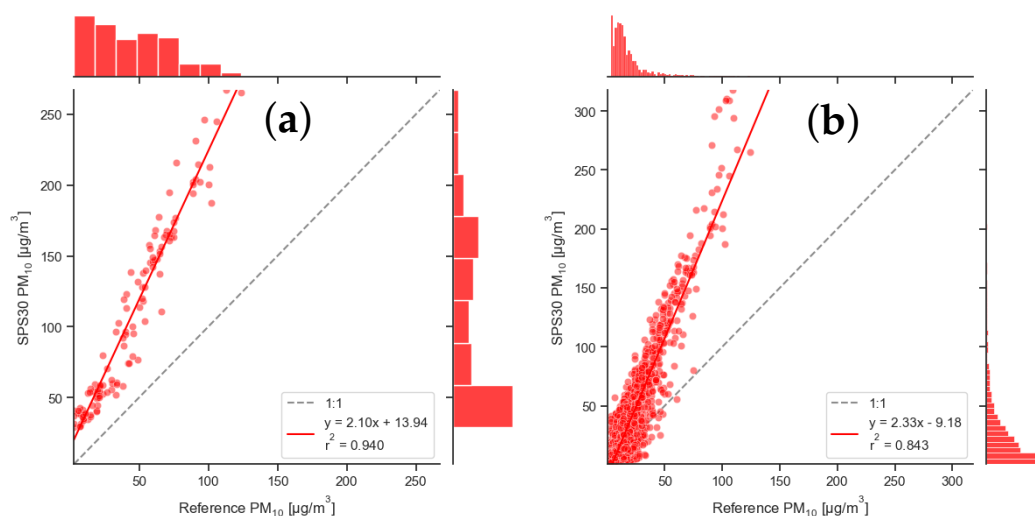


Figure 9. Simple linear regression of Sensirion SPS30 sensor response versus reference instrument (TEOM) for “Polish smog” episode S1 (a) compared with data for winter evaluation period (b). Histograms displayed adjacent to axes illustrate normalized frequency of measured concentration ranges within respective dataset.

3.3. LCS Performance During Saharan Dust Storm

During episode S2, a dramatic change in the response of SPS30 to dust particles was observed. In contrast to the winter evaluation period (with a positive bias of PM₁₀ readings), in the case of Saharan smog, PM₁₀ readings were negatively biased against the reference values. However, a nearly perfect agreement of the SPS30 response was found for PM₁ (see Figure 10). It is worth noting that the concentrations of carbon monoxide during the S2 episode were steadily below the limit of detection for the reference instrument ($[\text{CO}]_{\text{REF}} < 200 \mu\text{g}/\text{m}^3$).

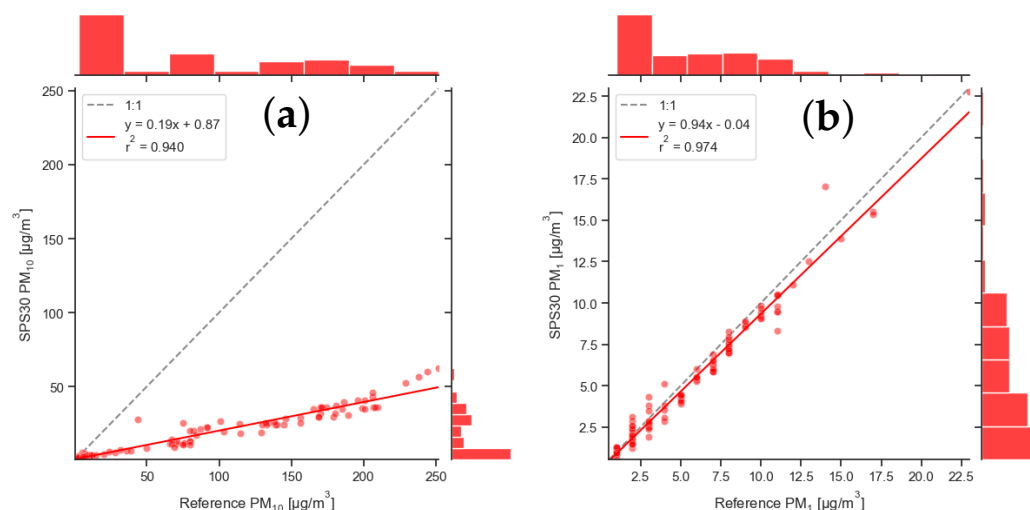


Figure 10. Simple linear regression of Sensirion SPS30 sensor response versus reference instrument (FIDAS) during spring “Saharan dust storm” episode S2. Performance shown for PM_{10} (a) and PM_1 (b). Histograms displayed adjacent to axes illustrate normalized frequency of measured concentration ranges within respective dataset.

4. Discussion

We first discuss our results regarding the response of the CO-B4 sensor and compare them with the observations of previous researchers. In the work of Camprodon et al. [9], a very high correlation ($R^2 > 0.8$) and low error ($RMSE < 0.1$ ppm) of CO measurements were observed during more than two months of CO-B4 sensor deployment. The sensor was found to behave linearly with respect to the CO concentrations and its decrease during the co-location period was negligible, which is quite consistent with our measurements. Our data obtained during the winter evaluation period (3 months) show a slightly higher coefficient of determination $R^2 \approx 0.9$ when re-calibration according to the Equation (1) is evaluated and compared with the reference data. A similar performance of this sensor is reported in Han et al. [12], evaluating an almost identical season with similar ranges of air pollutants, but with temperatures in the range 0–20 °C. Our co-location was carried out at much lower temperatures, while temperature correction following Equation (1) seemed to be less effective at extremely low ambient temperatures (below −10 °C) and high CO levels (see Figure 11). Conversely, slightly overestimated values of $[CO]_{LCS}$ were observed during the warmer days (with $t > 5$ °C). In the given case, we can attribute biased $[CO]_{LCS}$ values to a direct temperature effect on the sensing mechanism, i.e., a reduced rate of (electro-)chemical reactions, and the corresponding non-linearities.

On the other hand, as far as the influence of temperature on the response of the SPS30 sensor in our local conditions is concerned, we anticipate rather an indirect effect consisting in the change in particle size distribution due to the increased need for domestic and industrial heating at lower ambient temperatures.

This hypothesis is consistent with a number of previous publications, e.g., [19,20], mentioning in particular the work of Zareba et al. [20], who show a negative correlation between ambient temperature and the air pollution in an area close to our co-location site. Their study confirms that in moderate climate zones with coal burning as the primary source of air pollution, temperature is the most significant factor influencing monthly average PM_{10} concentrations.

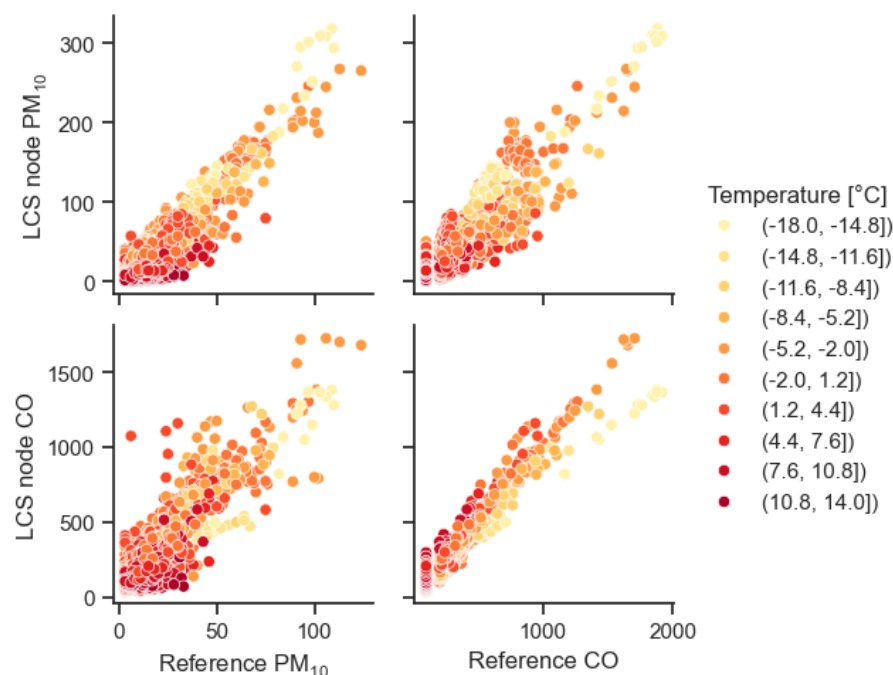


Figure 11. Correlation of reference measurements and LCS response during the winter evaluation period and the effect of ambient temperature on sensor performance (shown by the color of the data point).

As in the case of our co-location site, many AQM stations in the region covered by this paper are not yet equipped with reference instruments for measuring fine PM fractions. Moreover, the air quality criteria recommended by the WHO, EU, or local authorities for declaring a smog alert situation usually take into account PM_{10} concentrations or rarely $PM_{2.5}$. Therefore, our main motivation was to find a solution to reliably determine PM_{10} values based on LCS data.

Below, we briefly summarize some of the findings from previous studies on the performance of SPS30 sensors, in particular on their reliability in measuring fine and coarse PM concentration.

In a study by Roberts et al. [21], co-locating SPS30 with regulatory methods, they achieved an average bias adjusted $R^2 = 0.75$ for 24 h averages and 0.57 for 1 h averages, suggesting reasonable accuracy in real-time monitoring. The mean bias error was minimal, indicating that the SPS30 provided reliable data for $PM_{2.5}$ levels.

According to Kuula et al. [22], the SPS30 sensor is suitable to be used for measuring PM_1 particles when $R^2 = 0.91$, indicating high accuracy and consistency. Whereas for $PM_{2.5}$ particles, this value was 0.83, for PM_{10} particles, it was 0.12, indicating low measurement reliability and that sensor is not suitable for larger particle sizes.

Vogt et al. [23] also confirm that the SPS30 sensor is mostly accurate and reliable for PM_1 particles with $R^2 = 0.94$. For $PM_{2.5}$ particles, the R^2 value was around 0.73. The results for PM_{10} particles indicate a higher value ($R^2 = 0.46$) compared to the results of Kuula et al. [22], yet the sensor is still not suitable for practical AQM applications.

Molino Ruada et al. [15] confirmed the trend of the SPS30 sensor being able to measure PM_1 particles with a high accuracy of $R^2 = 0.93$. As the particle size increases, the accuracy of the sensor decreases, yielding $R^2 = 0.72$ for $PM_{2.5}$ and $R^2 = 0.23$ for PM_{10} , respectively.

The physical explanation for the unreliable measurement of larger particles is related to the design of optically based LCSs and the principle of their operation (i.e., light scattering). Above all, shortened viewing angles, losses occurring during particle intake and also differences in particle shape and refractive index need to be taken into account as well as the effect of humidity and sensor aging when these LCSs are exposed to realistic outdoor conditions.

Considering these findings together with the results of our LCS node measurements against the reference data, we can conclude that the SPS30 provides a reliable response to fine dust particles, especially PM_{10} , even under Saharan dust storm conditions. The PM_{10} readings from the SPS30 sensor according to its original calibration (i.e., factory setting) are burdened with a systematic bias, whose trend (negative or positive) depends on the type of smog situation. Therefore, to conclude this discussion, let us take a closer look at the size-resolved histogram of the PM volume concentration distribution obtained from the OPC-N3 sensor on days with maximum PM_{10} concentration in the case of S1 and S2 episodes (see Figure 12). The difference in particle size resolution is noticeable, with both data showing significant bimodality. In the case of the Polish smog (S1), the total volume is clearly dominated by PM_{10} . On the other hand, in the case of the Saharan dust storm (S2), particles with aerodynamic diameter $D_p \approx 4 \mu\text{m}$ have the highest volume concentration from the total PM_{10} found in the size-resolved distribution.

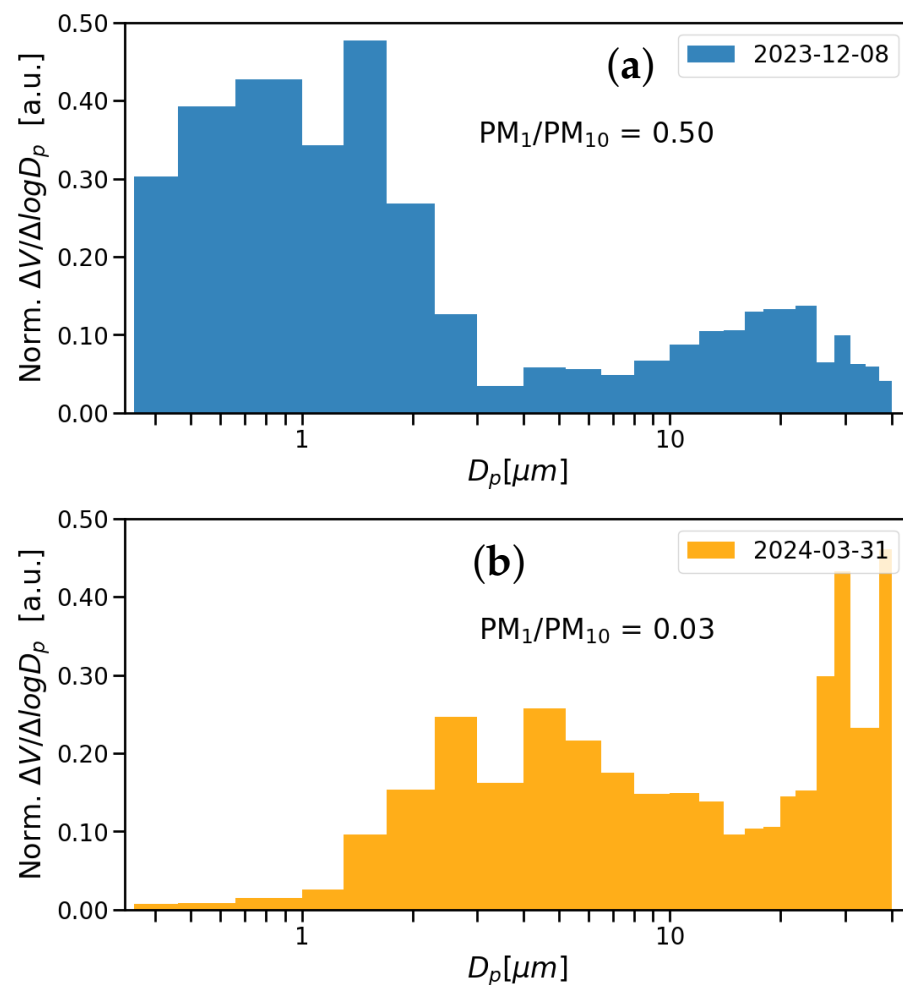


Figure 12. Size distribution of the normalized particle volume by bin of the Alphasense OPC-N3 sensor. The value of mass-weighted PM_{10}/PM_{10} ratio estimated from 24 h average on selected days during S1 (a) and S2 (b) episodes.

In an analogy to the recent work by Kaur and Kelly [24], we propose a strategy to derive PM_{10} concentrations from the biased PM-LCS response based on correction factors obtained from the OPC-N3 sensor working in concert. Further, we use Equations (3) and (4), which can be used to adjust slopes $a_{SLR,S1}$ and $a_{SLR,S2}$, respectively, to the ideal value $a_{COR} \approx 1$. Then, we can use the inverse estimation in order to determine that the calibration

of SPS30 is presumably carried out with the aerosol mixture having $[PM_1/PM_{10}]_{SPS,calibr} \approx 0.2 \pm 0.05$, which corresponds to common (traffic-related) air pollution in urban areas.

$$\frac{[PM_1/PM_{10}]_{OPC,S1}}{a_{SPS,S1}} = \frac{0.5}{2.1} = 0.23 \approx [PM_1/PM_{10}]_{SPS,calibr} \quad (3)$$

$$\frac{[PM_1/PM_{10}]_{OPC,S2}}{a_{SPS,S2}} = \frac{0.03}{0.19} = 0.16 \approx [PM_1/PM_{10}]_{SPS,calibr} \quad (4)$$

Therefore, the PM_{10} values measured by SPS30 are systematically biased if the actual $[PM_1/PM_{10}]$ values differ significantly from the $[PM_1/PM_{10}]_{SPS,calibr}$. In other words, it was proved that the biased SPS30 reading of PM_{10} could be roughly corrected using $[PM_1/PM_{10}]_{OPC}$ divided by a factor (0.2 ± 0.05). More precise corrections will only be possible after further analysis and experimentation.

4.1. Practical Applicability

This work represents a significant step towards strengthening the role of citizen science and democratizing environmental data in AQM, and it demonstrates the importance of academic support for these efforts as the current state of knowledge and technology is still rather prohibitive to the straightforward deployment of commercially available LCS systems in their default (factory-calibrated) setup. Therefore, a careful evaluation of LCS performance (in the form of co-location measurements) and a consideration of specific conditions of their deployment at local and regional levels before their practical application are inevitable.

In the framework of this work, we were able to explain the seasonal variability of the Sensirion SPS30 sensor response, and a correction method increasing the reliability of its PM_{10} response has established. According to our findings, we can exploit the strengths of the SPS30 sensor and overcome its previously reported limitations. A correction of its biased response can be expressed based on the fine-to-coarse particle ratio, e.g., as PM_1/PM_{10} evaluated from the OPC-N3 sensor. It was also found that an additional temperature correction needs to be estimated for the CO-B4 sensor to account for a biased response at extremely low temperatures.

Our future aim is to enhance the reliability of the regional AQM data when combining CAMS model predictions and LCS response by means of machine learning approaches employing parameterized (e.g., MLR or HDMR [25]) or non-parameterized methods [26].

4.2. Limitations

This study has several limitations, mainly due to the seasonal character and the influence of weather conditions relevant to the location and the winter season. It also specifically focuses only on the response of selected LCS systems integrated into a prototype node that is still under development. In our study, only individual pieces of the selected LCSs were tested and evaluated, thus not including the influence of inter-unit variability. Due to the duration of the co-location measurement, LCS aging factors were neglected.

5. Conclusions

This study evaluated the accuracy and reliability of a prototype low-cost sensor node for monitoring air pollution in the Moravian-Silesian Region, focusing on carbon monoxide (CO) and particulate matter (PM) during winter and transitional spring periods. The findings demonstrate that the selected low-cost sensors, particularly the CO-B4 and the SPS30 sensors, show high linearity in their readings under typical winter conditions. In accordance with Aim 1, a prototype LCS node was successfully developed and deployed for several months at the AQM station in Ostrava-Mariánské Hory. While searching for a suitable calibration procedure and methods, important properties of the LCS response during seasonal smog episodes were observed. However, systematic biases in PM_{10} measurements were identified during specific pollution episodes. These biases highlight the

need for improved calibration methods. Following Aim 2, this study investigated initial calibration adjustments using a back-estimation method based on the PM_1/PM_{10} ratio derived from the OPC-N3 sensor and demonstrated the potential for reducing bias and increasing sensor reliability under local conditions. Importantly, our findings reveal that, with appropriate calibration adjustments, the SPS30 sensor shows potential for quantitative PM_{10} measurement, even though previous studies, such as Molino-Ruada et al. [15], have raised concerns about its suitability for low-cost sensor (LCS) networks. Despite these concerns, our study suggests that by applying corrections derived from particle size distributions, the SPS30 sensor can be effectively used in LCS networks for air quality monitoring in regions with specific environmental challenges, such as the Moravian-Silesian Region. In addition to evaluating the performance of the prototype sensor node, our findings obtained by targeting Aim 3 offer potential for use in improving both the accuracy of LCS monitoring and the reliability of CAMS model predictions, particularly in relation to local air pollution episodes. Overall, this study highlights the potential of low-cost sensor networks, with appropriate calibration, to provide reliable air quality data in industrial regions like the Moravian-Silesian Region. Such networks could effectively supplement regulatory-grade monitoring systems. Future research will focus on enhancing sensor recalibration methods, particularly through the back-estimation method, and further exploring the integration of CAMS data to optimize the accuracy of low-cost air quality monitoring systems.

Author Contributions: V.N.: writing—original draft, resources, methodology, investigation, data curation, conceptualization. M.D.: writing—original draft, validation, methodology, investigation. P.B.: conceptualization, investigation, resources. V.K.: methodology, investigation, data curation. J.S. (Jiří Sléžka): software, investigation. P.P.: software, investigation. K.N.: investigation. M.B.: writing—original draft, visualization, investigation. R.L.: investigation. Š.B.: investigation. B.M.: investigation. M.V.: software, data curation, investigation. A.N.: software, data curation, investigation. M.L.: data curation, investigation. J.S. (Jan Suchánek): project administration, resources, investigation. H.C.: investigation. D.K.: data curation, investigation. J.W.: supervision, funding acquisition. All authors have read and agreed to the published version of the manuscript.

Funding: This research was funded from project no. SS03010139 of the Technology Agency of the Czech Republic and project No. 22-19812S funded by the Czech Science Foundation.

Institutional Review Board Statement: Not applicable.

Informed Consent Statement: Not applicable.

Data Availability Statement: The raw datasets and Python interactive notebooks used for the preparation of this paper are freely available in the Zenodo repository (<https://doi.org/10.5281/zenodo.13863368>), accessed on 1 October 2024.

Acknowledgments: We gratefully acknowledge the institutional support of the VSB-Technical University of Ostrava (the Faculty of Safety Engineering) via student project No. SP2024/044.

Conflicts of Interest: The authors declare no conflicts of interest.

Abbreviations

PM_1	particulate matter with diameter ≤ 1 micrometer
$PM_{2.5}$	particulate matter with diameter ≤ 2.5 micrometers
PM_{10}	particulate matter with diameter ≤ 10 micrometers
CO	carbon monoxide
CAMS	Copernicus Atmospheric Monitoring Service
VOCs	volatile organic compounds
O_3	ozone
LCS	low-cost sensor
AQM	air quality monitoring

EU	European Union
RMSE	root mean square error
RH	relative humidity
NDIR	nondispersive infrared
TEOM	tapered element oscillating microbalance
LoD	limit of detection
CSV	comma-separated value
MLR	multilinear regression
MAE	mean average error
GMT	Greenwich mean time
SLR	simple linear regression
atmospy	Python library for atmospheric data analysis
smpls-py	Python library for particle size distribution analysis
NO ₂	nitrogen dioxide
UV	ultraviolet radiation
r	Pearson correlation coefficient
[CO] _{LCS}	CO concentration measured by LCS
[CO] _{REF}	reference CO concentration
[CO] _{CAMS}	CO concentration from CAMS model
[PM ₁₀] _{REF}	reference PM ₁₀ concentration
S1	smog episode 1
S2	smog episode 2
R ²	coefficient of determination
ANN	artificial neural network
HDMR	high-dimensional model representation
LoRaWAN	long-range wide-area network
ASA	acrylonitrile styrene acrylate (3D printing material)
MQTT	message queuing telemetry transport

Appendix A. LCS Node Design and Data Management

Appendix A.1. Hardware Description

The LCS sensor node is designed as a modular system with three interconnected printed circuit boards (PCBs), each serving a specific function: control and communication, sensor interface, and power management.

The Control and Communication Board houses the LilyGo TTGO LoRa32 T3 v1.6 with 868MHz microcontroller module, featuring the ESP32. This board manages data collection and communication, utilizing Wi-Fi (employed within this work) and LoRaWAN (optional). It operates primarily at 3.3V, with voltage regulators and DC-DC converters ensuring stable power supply for consistent performance.

The Power Management Board distributes power across the system and supports multiple power input options, including DC from the grid (employed within this work), lithium-ion batteries, and 6V lead-acid batteries (optional). This board includes DC-DC converters and voltage regulators to step down input voltages to the necessary levels. It also integrates a slot for NEO-6M GPS module for geolocation, providing real-time position data alongside environmental measurements.

The Sensor Interface Board integrates individual sensors, including particulate matter (Alphasense OPC-N3 and Sensirion SPS30). It also features an Analog-to-Digital Converter ADS1115 to process signals from analog Alphasense type B sensors. Stable voltage of 3.5V is provided for Individual Sensor Boards as required for measurement accuracy.

The interconnection of these PCBs ensures seamless communication and power distribution, contributing to the mechanical stability of the sensor node and simplifying assembly and future modifications.

Additionally, a custom-designed enclosure for the sensor node was developed and manufactured using MDF 3D printing technology. The material chosen for the enclosure is ASA (Acrylonitrile Styrene Acrylate), which offers excellent weather resistance and durability. The enclosure not only protects the sensors from external elements but also ensures proper airflow for accurate measurements. A 3D model of the sensor node’s enclosure is shown in Figure A1.

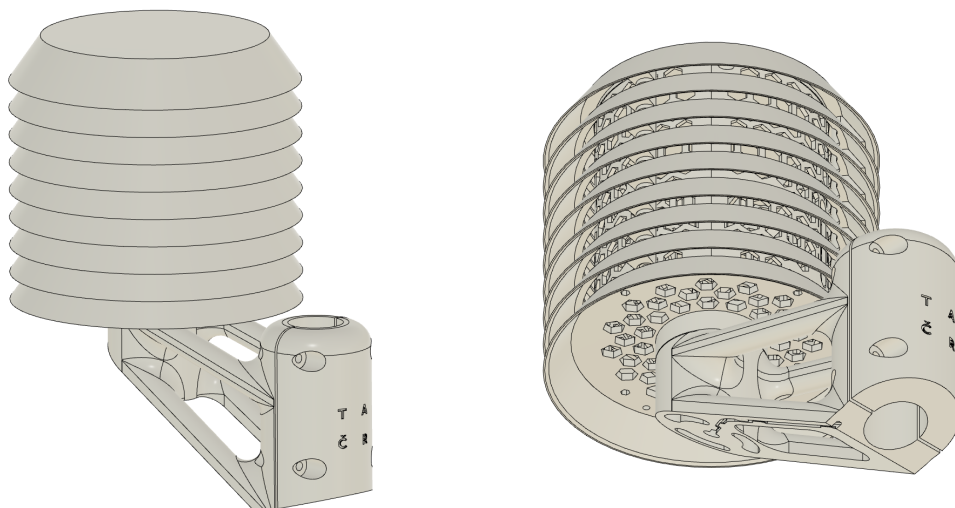


Figure A1. Rendered 3D model of the LCS node enclosure.

Appendix A.2. Datalogging

As illustrated in the Figure A2 data logging from LCS node is a multistep process. Sensor node is equipped with an ESP32 microcontroller, which gathers data at regular intervals. This data is transmitted using Wi-Fi via the MQTT protocol, specifically through the Mosquitto MQTT broker, which publishes the data to designated topics. Telegraf, configured to listen to these MQTT topics, subscribes to the relevant data streams and stores the incoming information in an InfluxDB database.

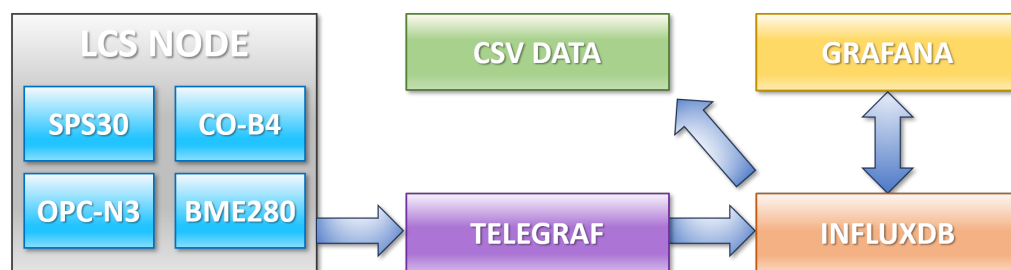


Figure A2. Schematic representation of the data logging framework.

To make this data accessible and interpretable, Grafana connects to the InfluxDB database and visualizes the data on customizable dashboards. Selected datasets from co-location measurement are resampled with 10-min temporal resolution and automatically transferred to CSV format in monthly intervals. These data can be accessed from publicly available web interface SOASENSE (<https://soasense.vsb.cz>, accessed on 1 October 2024)

References

1. Svozilík, V.; Svozilíková Krakovská, A.; Bitta, J.; Jančík, P. Comparison of the Air Pollution Mathematical Model of PM10 and Moss Biomonitoring Results in the Třitva Region. *Atmosphere* **2021**, *12*, 656. [CrossRef]
2. Volná, V.; Hladký, D.; Seibert, R.; Krejčí, B. Transboundary Air Pollution Transport of PM10 and Benzo[a]pyrene in the Czech–Polish Border Region. *Atmosphere* **2022**, *13*, 341. [CrossRef]
3. Volná, V.; Seibert, R.; Hladký, D.; Krejčí, B. Identification of Causes of Air Pollution in a Specific Industrial Part of the Czech City of Ostrava in Central Europe. *Atmosphere* **2024**, *15*, 177. [CrossRef]
4. Świączkowski, M.; Dobrzycki, S.; Kuźma, Ł. Multi-City Analysis of the Acute Effect of Polish Smog on Cause-Specific Mortality (EP-PARTICLES Study). *Int. J. Environ. Res. Public Health* **2023**, *20*, 5566. [CrossRef] [PubMed]
5. Wielgoński, G.; Czerwińska, J. Smog Episodes in Poland. *Atmosphere* **2020**, *11*, 277. [CrossRef]
6. Castell, N.; Dauge, F.R.; Schneider, P.; Vogt, M.; Lerner, U.; Fishbain, B.; Broday, D.; Bartonova, A. Can commercial low-cost sensor platforms contribute to air quality monitoring and exposure estimates? *Environ. Int.* **2017**, *99*, 293–302. [CrossRef]
7. Gabrys, J. Planetary health in practice: Sensing air pollution and transforming urban environments. *Hum. Soc. Sci. Commun.* **2020**, *7*, 35. [CrossRef]
8. Mahajan, S.; Chung, M.K.; Martinez, J.; Olaya, Y.; Helbing, D.; Chen, L.J. Translating citizen-generated air quality data into evidence for shaping policy. *Hum. Soc. Sci. Commun.* **2022**, *9*, 122. [CrossRef]
9. Camprodon, G.; González, Ó.; Barberán, V.; Pérez, M.; Smári, V.; de Heras, M.Á.; Bizzotto, A. Smart Citizen Kit and Station: An open environmental monitoring system for citizen participation and scientific experimentation. *HardwareX* **2019**, *6*, e00070. [CrossRef]
10. Giordano, M.R.; Malings, C.; Pandis, S.N.; Presto, A.A.; McNeill, V.; Westervelt, D.M.; Beekmann, M.; Subramanian, R. From low-cost sensors to high-quality data: A summary of challenges and best practices for effectively calibrating low-cost particulate matter mass sensors. *J. Aerosol Sci.* **2021**, *158*, 105833. [CrossRef]
11. Cross, E.S.; Williams, L.R.; Lewis, D.K.; Magoon, G.R.; Onasch, T.B.; Kaminsky, M.L.; Worsnop, D.R.; Jayne, J.T. Use of electrochemical sensors for measurement of air pollution: correcting interference response and validating measurements. *Atmos. Meas. Tech.* **2017**, *10*, 3575–3588. [CrossRef]
12. Han, P.; Mei, H.; Liu, D.; Zeng, N.; Tang, X.; Wang, Y.; Pan, Y. Calibrations of Low-Cost Air Pollution Monitoring Sensors for CO, NO₂, O₃, and SO₂. *Sensors* **2021**, *21*, 256. [CrossRef] [PubMed]
13. Hagan, D.H.; Isaacman-VanWertz, G.; Franklin, J.P.; Wallace, L.M.M.; Kocar, B.D.; Heald, C.L.; Kroll, J.H. Calibration and assessment of electrochemical air quality sensors by co-location with regulatory-grade instruments. *Atmos. Meas. Tech.* **2018**, *11*, 315–328. [CrossRef]
14. Liang, L.; Daniels, J. What Influences Low-cost Sensor Data Calibration?—A Systematic Assessment of Algorithms, Duration, and Predictor Selection. *Aerosol Air Qual. Res.* **2022**, *22*, 220076. [CrossRef]
15. Molina Rueda, E.; Carter, E.; L'Orange, C.; Quinn, C.; Volckens, J. Size-Resolved Field Performance of Low-Cost Sensors for Particulate Matter Air Pollution. *Environ. Sci. Technol. Lett.* **2023**, *10*, 247–253. [CrossRef]
16. METEO FRANCE; Institut National de L'environnement Industriel et des Risques (INERIS); Aarhus University; Norwegian Meteorological Institute (MET Norway); Jülich Institut für Energie- und Klimaforschung (IEK); Institute of Environmental Protection—National Research Institute (IEP-NRI); Koninklijk Nederlands Meteorologisch Instituut (KNMI); Nederlandse Organisatie voor Toegepast-Natuurwetenschappelijk Onderzoek (TNO); Swedish Meteorological and Hydrological Institute (SMHI); Finnish Meteorological Institute (FMI); et al. CAMS European Air Quality Forecasts, ENSEMBLE Data. 2022. Available online: <https://ads.atmosphere.copernicus.eu/datasets/cams-europe-air-quality-forecasts?tab=overview> (accessed on 1 August 2024).
17. Varga-Balogh, A.; Leelőssy, Á.; Lagzi, I.; Mészáros, R. Time-Dependent Downscaling of PM2.5 Predictions from CAMS Air Quality Models to Urban Monitoring Sites in Budapest. *Atmosphere* **2020**, *11*, 669. [CrossRef]
18. Chen, Y.; Zang, L.; Chen, J.; Xu, D.; Yao, D.; Zhao, M. Characteristics of ambient ozone (O₃) pollution and health risks in Zhejiang Province. *Environ. Sci. Pollut. Res.* **2017**, *24*, 27436–27444. [CrossRef]
19. Zhang, X.; Zhou, B.; Li, Z.; Lin, Y.; Li, L.; Han, Y. Seasonal Distribution of Atmospheric Coarse and Fine Particulate Matter in a Medium-Sized City of Northern China. *Toxics* **2022**, *10*, 216. [CrossRef]
20. Zareba, M.; Weglinska, E.; Danek, T. Air pollution seasons in urban moderate climate areas through big data analytics. *Sci. Rep.* **2024**, *14*, 3058. [CrossRef]
21. Roberts, F.; Van Valkinburgh, K.; Green, A.; Post, C.J.; Mikhailova, E.A.; Commodore, S.; Pearce, J.L.; Metcalf, A.R. Evaluation of a new low-cost particle sensor as an internet-of-things device for outdoor air quality monitoring. *J. Air Waste Manag. Assoc.* **2022**, *72*, 1219–1230. [CrossRef]
22. Kuula, J.; Mäkelä, T.; Aurela, M.; Teinilä, K.; Varjonen, S.; González, Ó.; Timonen, H. Laboratory evaluation of particle-size selectivity of optical low-cost particulate matter sensors. *Atmos. Meas. Tech.* **2020**, *13*, 2413–2423. [CrossRef]
23. Vogt, M.; Schneider, P.; Castell, N.; Hamer, P. Assessment of Low-Cost Particulate Matter Sensor Systems against Optical and Gravimetric Methods in a Field Co-Location in Norway. *Atmosphere* **2021**, *12*, 961. [CrossRef]
24. Kaur, K.; Kelly, K.E. Performance evaluation of the Alphasense OPC-N3 and Plantower PMS5003 sensor in measuring dust events in the Salt Lake Valley, Utah. *Atmos. Meas. Tech.* **2023**, *16*, 2455–2470. [CrossRef]

25. Bittner, A.S.; Cross, E.S.; Hagan, D.H.; Malings, C.; Lipsky, E.; Grieshop, A. Performance Characterization of Low-cost Air Quality Sensors for Off-grid Deployment in Rural Malawi. *Atmos. Meas. Tech.* **2022**, *15*, 3353–3376. [[CrossRef](#)]
26. Topalović, D.B.; Davidović, M.D.; Jovanović, M.; Bartonova, A.; Ristovski, Z.; Jovašević-Stojanović, M. In search of an optimal in-field calibration method of low-cost gas sensors for ambient air pollutants: Comparison of linear, multilinear and artificial neural network approaches. *Atmos. Environ.* **2019**, *213*, 640–658. [[CrossRef](#)]

Disclaimer/Publisher’s Note: The statements, opinions and data contained in all publications are solely those of the individual author(s) and contributor(s) and not of MDPI and/or the editor(s). MDPI and/or the editor(s) disclaim responsibility for any injury to people or property resulting from any ideas, methods, instructions or products referred to in the content.